

Thermal Patterns in Peripheral Regions of Breast during Different Stages of Development

Akshara Makrariya* and Neeru Adlakha

Department of Applied Mathematics and Humanities, Sardar Vallabhbhai National Institute of Technology, Surat, Gujarat 395007, India

*Corresponding author: Akshara Makrariya, Department of Applied Mathematics and Humanities, Sardar Vallabhbhai National Institute of Technology, Surat, Gujarat 395007, India, Tel: 0261 225 9571; E-mail: aksharahul@gmail.com

Received date: September 25, 2016; Accepted date: November 09, 2016; Published date: November 16, 2016

Copyright: © 2016 Makrariya A, et al. This is an open-access article distributed under the terms of the Creative Commons Attribution License, which permits unrestricted use, distribution and reproduction in any medium, provided the original author and source are credited.

Abstract

Background: Mathematical modelling of bio thermal processes is widely used to enhance the quantitative understanding of thermoregulation system of human body organs. This quantitative knowledge of thermal information of various human body organs can be used for developing clinical applications. In the past the investigators have studied thermal distribution in hemispherical shaped human breast in presence of spherical shaped tumor. The shape and size of the breast as well as tumor may also affect thermal distribution which can have serious implications in thermography. In the present paper a model of thermal disturbances in peripheral regions of ellipsoidal shaped breast for two dimensional steady state case. The modelling study will provide biomedical scientist vital insights of thermal changes occurring due to shape and size of breast which can influence the development of protocols of thermography for diagnosis and treatment of tumors in women's breast.

Method: We have incorporated the significant parameters like blood flow, metabolic activity and thermal conductivity in the thermal model for normal and malignant tissues. The controlled metabolic activity has been incorporated for normal tissues. The peripheral regions of breast are divided into three major layers mainly epidermis, dermis and sub dermal tissues. The outer surface of the breast is assumed to be exposed to the environment and the heat loss takes place by conduction, convection, radiation and evaporation. The finite element approach is employed to obtain the solution.

Results: By selecting appropriate model parameters we have shown the spatial thermal variation in different stages of breast according to their shapes which could be replicated by the proposed model.

Conclusions: The proposed model was successfully employed to study the impact of different sizes and shapes in peripheral regions of elliptical shaped woman's breast. The proposed model is more realistic in terms of shape and size of woman's breast in comparison to earlier models reported in the literature. The changes in slope of the thermal curves at the junctions of various peripheral layers are due to the non homogenous nature of the region.

Keywords: Thermal patterns; Stages of breast development; Semi elliptical shaped breast; Finite element method; Coaxial elliptical sectoral element

Introduction

The temperature changes within the human body in relation to disease have been recognized for many centuries. In particular the elevated body temperature has been used as an indicator of illness and often as an indicator of the progression of a disease. The medical and clinical practitioners use temperature as an indicator of tissue response under various clinical and health situations [1-3]. In order to understand the relation of tissue temperature with disease, it is of crucial interest to understand the thermoregulation of human body. The human body maintains its body core temperature at a uniform temperature i.e., 37°C by maintaining balance between metabolic heat generation in the body tissues and heat loss to the environment from the skin surface. The skin and subdermal tissues (peripheral) region is the medium for heat transport from body core to the body surface. This peripheral region is also known as peripheral region is a non homogeneous medium and consists of three layers namely epidermis,

dermis and sub dermal tissues [4,5]. The dermis is made up of matted masses of connective tissues, elastic fibres, blood vessels, lymphatic and nerves. There are no blood vessels in the epidermis. The population density of blood vessels in the dermis is very thin near the interface of epidermis, but it increases gradually and becomes almost uniform in the sub dermal part [6].

Apart from the biophysical parameters like thermal conductivity, blood flow, and metabolic activity, the structure, shape and size of the body organs also influence this tissue temperature of the human or animal body. The shape, size and structure of the breast vary depending on the stages of development, age, community etc. [7]. The female breast is made up of glandular, fatty, and fibrous tissues. There is a layer of fatty tissue that surrounds the breast glands and runs throughout the entire breast. This fat gives breasts their soft consistency, size and shape. Inside the glandular tissues are the functional parts of the breast.

The development of breast takes place in five stages as shown in Figure 1. In the first stage only the tip of the nipple is the raised part and otherwise it is flat. It is the childhood stage i.e., less than 7 to 8 years, before puberty begins and the breasts have not started to

develop. In the second stage of development the buds appear, breast and nipple are raised, and the areola (dark area of skin that surrounds the nipple) enlarges. This stage occurs during the age of 8 to 13 years. In the third stage breasts are slightly larger with glandular breast tissue present in them. Girls usually reach this stage when they are 12 to 14 years old. The areola and nipple become raised and form a second mound above the rest of the breast in the fourth stage of development [8]. Girls often reach this stage when they are 12 to 15 years old and many girls reach stage 4 at ages that are outside this range. Finally in the fifth stage mature adult breast is developed during the age of 15 to 18 years and in this stage the breast becomes rounded and only the nipple is raised.

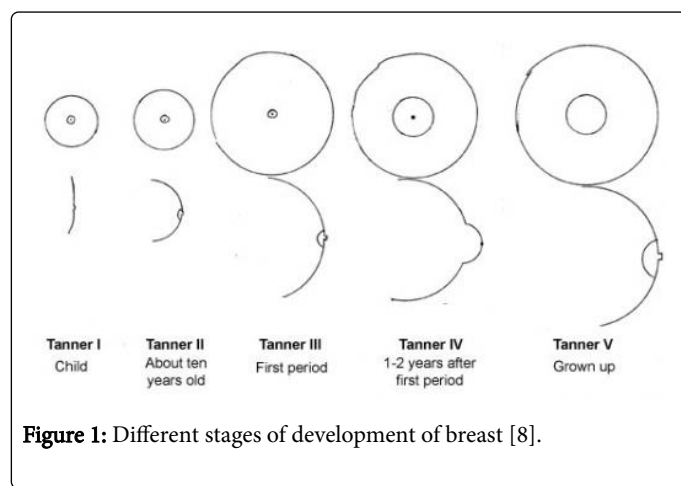


Figure 1: Different stages of development of breast [8].

The shape and size of a woman's breast keeps changing during her life and depends completely on genetic factors, climate conditions, diet, lifestyle and the kind of support they are given during and after development. It has been found that the shape and size of the right and left breasts for no women are identical. In fact it is quite common that one breast will be larger than the other.

Several investigations have been made by various research workers [4-6,9-11] to study one dimensional heat flow in flat shaped human organs. Also some attempts have been made [12,13-15] to study heat flow in dermal regions of flat and cylindrical human organs for two dimensional cases. Attempts [16-18] have also been made to study thermal patterns in skin and subcutaneous tissues involving abnormalities like tumour in flat shaped human organs for one and two dimensional cases. But very little attention has been paid to the study of heat flow in spherical shaped human organs. The thermoregulation in human head has been investigated [19] under cold environment using finite element method. The thermal modelling of women breast under normal environmental conditions has been carried out by researchers to study [20,21] relationships among various biophysical parameters. Theoretical investigations [22-24] have also been carried out to study effect of tumor in deep tissues of women's breast on the surface temperature of the breast. The semi numerical [1-3] and finite element models are [1-3,25,26-29] reported in the literature for the study of thermal patterns in cylindrical and irregular tapered shaped human organs like limbs for two and three dimensional cases with and without tumors. Recently [30-32] have developed a two dimensional finite element model to study thermal patterns in peripheral regions of hemispherical shaped human breast for normal and breast tumor.

From the literature survey it is observed that no attempt is reported till date to study thermal patterns in elliptical shaped human breast. Further no research workers have taken into account the size and shape of the breast depending on the various stages of development of the breast. In the present study a finite element model has been developed to study thermal patterns in peripheral region of semi elliptical shaped human breast under different stages of development for a two dimensional steady state case. The effect of shape and size of breast on thermal patterns in the peripheral region of the breast is analysed.

Mathematical Model

The partial differential equation for heat flow in the peripheral region which was given by [33]:

$$(\rho c) \frac{\partial T}{\partial t} = \nabla \cdot (K \nabla T) + m_b c_b (T_A - T) + S \quad (1)$$

Where the effect of blood flow and metabolic heat generation is given by the terms $m_b c_b (T_b - T)$ and S respectively. Here K =Thermal conductivity of tissue, m_b =Blood mass flow rate, c_b =Specific heat of blood, T_b =Arterial blood temperature, T =Tissue temperature at position r measured perpendicularly from the skin surface, c = specific heat of the tissues at time t , S =Rate of metabolic heat generation, ρ =Tissue density. We consider $T_A = T_b$ =Body core temperature, as the blood flows in arteries from the body core at body core temperature.

The human breast is assumed to be ellipsoidal in shape with upper semi ellipsoidal region projecting out from the trunk of the body and lower semi ellipsoidal portion is considered to be a part of the body core. The deep tissues of breast consisting of muscles, glands and fat are considered to be a part of the breast core. Above the breast core is the peripheral region.

The equation (1) for thermal patterns in living tissues for a two dimensional steady state case in elliptical coordinates is given by:

$$\frac{1}{d^2 (\sinh^2 \mu + \sin^2 \nu)} \left[K \frac{\partial}{\partial \mu} \left(\frac{\partial T}{\partial \mu} \right) + K \frac{\partial}{\partial \nu} \left(\frac{\partial T}{\partial \nu} \right) \right] + m_b c_b (T_A - T) + S = 0 \quad (2)$$

Here d is the eccentricity of elliptical layer, μ and ν are the radial and angular coordinates for the ellipsoidal shaped human breast.

The outer surface of the region is exposed to the environment and heat loss at this surface takes place mainly due to convection, radiation, and evaporation [9,10]. Hence the boundary condition imposed at the outer surface is given by:

$$-k \frac{\partial T}{\partial r} = h(T - T_a) + LE \text{ at } \mu = \mu_3, \nu \in (0, \pi) \quad (3)$$

Where, h =heat transfer coefficient, T_a =atmospheric temperature, L =latent heat of evaporation, E =Rate of evaporation & represents flux normal to the skin surface.

The condition at the inner boundary is imposed for two cases as given below.

Case I boundary condition

At medium and higher atmospheric temperatures the inner boundary is maintained at uniform body core temperature T_b . Thus inner boundary is assumed to be at constant temperature T_b . Hence the condition at inner boundary is given by:

$$T(\mu_0, \nu) = T_b \text{ at } \mu = \mu_0 \quad (4)$$

Where μ_0 is the radial position of inner boundary.

Case II boundary condition

At low atmospheric temperatures, the core temperature of the human breast is variable along angular direction ν . This is because the warm blood flows in arteries at 37°C from the core of the trunk to the core of the human breast and the same blood reaching extreme [21] parts of the breast cools down and returns back from extremities of the breast through veins at lower temperature than the body core temperature. Hence the following boundary condition is imposed.

$$T(\mu_0, \nu) = F(\nu) \quad (5)$$

$$F(\nu) = a_1 + a_2\nu + a_3\nu^2 \quad (6)$$

Here a_1, a_2 and a_3 are constants.

The value of a_1, a_2, a_3 are found by using the conditions

$$T(\mu_0, \nu) = \alpha \text{ at } \nu = 0 \quad (7)$$

$$T(\mu_0, \nu) = \beta \text{ at } \nu = \pi/2 \quad (8)$$

$$T(\mu_0, \nu) = \gamma \text{ at } \nu = \pi \quad (9)$$

Hence the value of α, β and γ are constants, which can be assigned the values based on the temperature at selected points of the core of human breast.

The peripheral region of the breast is divided into the three layers namely epidermis, dermis and subcutaneous tissues, which are considered to be elliptic with eccentricity d_1, d_2 and d_3 respectively. The coaxial elliptical sectoral elements have been employed to discretize the region as given in Figure 2. The whole region is divided into the 18 elements. This division of each layer into different number of elements of different sizes has been done in order to match with the geometry and physiological properties of the region [33].

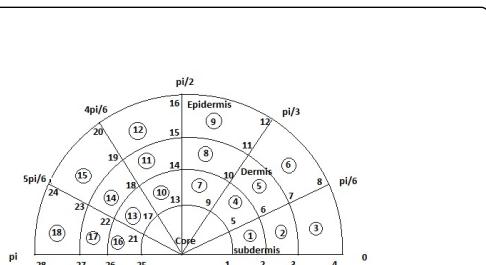


Figure 2: Finite element discretization of human breast using coaxial elliptical sectoral element.

The equation (2) along with the boundary conditions (3) and (4) is written in the variational form [20] as given below:

$$I^{(e)} = \frac{1}{2} \int_{\nu_i}^{\nu_j} \int_{\mu_i}^{\mu_j} \left[K^{(e)} \left\{ \left(\frac{\partial T^{(e)}}{\partial \mu} \right)^2 + \left(\frac{\partial T^{(e)}}{\partial \nu} \right)^2 \right\} + A_1^{(e)} \left\{ m_b c_b (T_A^{(e)} - T)^2 - 2S^{(e)} T^{(e)} \right\} \right] d\mu d\nu + \frac{\lambda^{(e)}}{2} \int_{\nu_j}^{\nu_k} A_1^{(e)} \left\{ h (T^{(e)} - T_a)^2 + 2LET^{(e)} \right\} d\nu \text{ for } e = 1(1)18 \quad (10)$$

Here $A_1^{(e)} = d^{(e)2} (\sinh^2 \mu^{(e)} + \sin^2 \nu^{(e)})$, μ_i and μ_j are boundaries of the eth element $K^{(e)}, M^{(e)}, S^{(e)}, T_A^{(e)}$ and $T^{(e)}$ denote the values of K, M, S, T_A and T respectively in the eth layer [25]. $\lambda^{(e)}=1$ for elements along the surface and $\lambda^{(e)}=0$ for all the elements which are not along the outer surface.

The following bilinear shape function for variation of temperature within each element has been taken as [6].

$$T^{(e)} = c_1^{(e)} + c_2^{(e)}\mu + c_3^{(e)}\nu + c_4^{(e)}\mu\nu \quad (11)$$

Where $c_1^{(e)}, c_2^{(e)}, c_3^{(e)}$ and $c_4^{(e)}$ are constants for the eth element.

Using above values of parameters the integral (10) are evaluated and assembled as follows:

$$I = \sum_{i=1}^n I_i^{(e)} \quad (12)$$

This leads to a system of linear algebraic equations given below:

$$[X]_{28 \times 28} [\bar{T}]_{28 \times 1} = [Y]_{28 \times 1} \quad (13)$$

Here, $\bar{T} = [T_1 \ T_2 \ T_3 \ \dots \ T_{28}]$. X is the system matrix of order 28×28 and Y is system vector of order 28×1 . The two types of boundary conditions (4) and (5) are incorporated at the inner core of the breast in these systems of equations (13). The Gauss elimination method has been used to obtain the solution of (13). A computer program in MATLAB is developed to find numerical solution to the entire problem. The time taken for simulation is nearly 2 minutes on Core(TM) i3 CPU M 330 @ 2.13 GHz processing speed and 3 GB memory.

Numerical Result and Discussion

Numerical result

The numerical results are obtained by using the values of physical and physiological constants [11,12] as given in Table 1.

Atmospheric temperature Ta (°C)	Mmax=(mbcb)/max=m Cal/cm ³ -min deg.C	Smax=s cal/cm ³ min	E=gm/cm ² min
15°C	0.003	0.0357	0
23°C	0.018	0.018	0.0, 0.24 × 10 ⁻³ , 0.48 × 10 ⁻³
33°C	0.315	0.018	0.0, 0.24 × 10 ⁻³ , 0.48 × 10 ⁻³ , 0.72 × 10 ⁻³

Table 1: Values of parameters [16].

The simulation was performed for N=18 elements initially. Then again the simulation was performed by taking N=36, 54 and 72 elements. We get breast surface temperature as 34.1566 for the model with N=18 elements and breast surface temperature 34.1576, for the model with N=72 elements. The error is [(34.1576-34.1566)/34.1576]*100 which works out to be 27 × 10⁻⁶ % only. For better clarity, we take only the ratio of four decimal points (0.1566/0.1576)*100=99.89% and call this term as confidence level. A confidence level of 100 implies that a saturation point has been reached. In this work, we have used N=18 elements as the number of elements in our model as we can safely say that results are mesh insensitive at this number.

The expression for nodal information is given below:

Radial coordinates:- $\mu_i = r_{k-1}$ for $i=k+4j : j=0 (1)7$ and $k=1 (1) 4$

The constants r_i ($i=0(1)3$) can be assigned any value depending upon particular sample of tissue layers under study. The results are computed for following four sample layers of peripheral region of breast based on stage II to V respectively as given below:

Set: 1 $r_0=2.0$ cm, $r_1=2.5$ cm, $r_2=2.9$ cm. $r_3=3.1$ cm, For Stage II

Set: 2 $r_0=3.0$ cm, $r_1=3.5$ cm, $r_2=3.9$ cm. $r_3=4.1$ cm, For Stage III

Set: 3 $r_0=6.0$ cm, $r_1=6.5$ cm, $r_2=6.9$ cm. $r_3=7.1$ cm, For Stage IV

Set: 4 $r_0=10.0$ cm, $r_1=10.5$ cm, $r_2=10.9$ cm. $r_3=11.1$ cm, For Stage V

Eccentricity is given by:

$d_i = d_{k-1}$ for $i=k+4j : j=0 (1)7$ and $k=1 (1) 4$

For any ellipse we can define a number of related eccentricities depending upon sample of a human organ under study. The following sets of eccentricities have been taken as a particular case:

Set: 1 $d_1=0.0030$ cm, $d_2=0.0028$ cm, $d_3=0.0025$ cm.

Set: 2 $d_1=0.0030$ cm, $d_2=0.0028$ cm, $d_3=0.0025$ cm.

Set: 3 $d_1=0.0030$ cm, $d_2=0.0028$ cm, $d_3=0.0025$ cm.

Set: 4 $d_1=0.0030$ cm, $d_2=0.0028$ cm, $d_3=0.0025$ cm.

Here d_1 represents the eccentricity of the breast core. The eccentricities d_2 and d_3 are computed values based on d_1 . For case II boundary condition the following values are assigned to the constants α , β and γ

$$\alpha = 37^\circ C, \beta = 36^\circ C, \gamma = 37^\circ C$$

The numerical results have been computed and graphs are plotted for the different cases of atmospheric temperatures and different values of rate of evaporation [9-11].

Discussion

Graphs have been plotted for thermal patterns along radial and angular direction which are shown in Figures 3 to 26. The Figures 3 to 18 are for the case I boundary condition and Figures 19 to 26 are for case II boundary condition.

Case I boundary condition

Figures 3 to 6 show thermal patterns for $T_a=23^\circ C$, $E=0.48 \times 10^{-3}$ gm/cm²min case I, eccentricity of breast core $d_1=0.0030$ for the stages II, III, IV and V of breast development respectively. In these Figures it is observed that the slope of the curve changes at the junctions of the different layers in the region.

In Figure 6 for stage V the fall in temperature is more as compared to Figure 3 for stage II.

Figures 7 to 10 show thermal patterns for $T_a=33^\circ C$, $E=0.48 \times 10^{-3}$ gm/cm²min case I, eccentricity of breast core $d_1=0.0030$ and for the stages II, III, IV and V of breast development respectively.

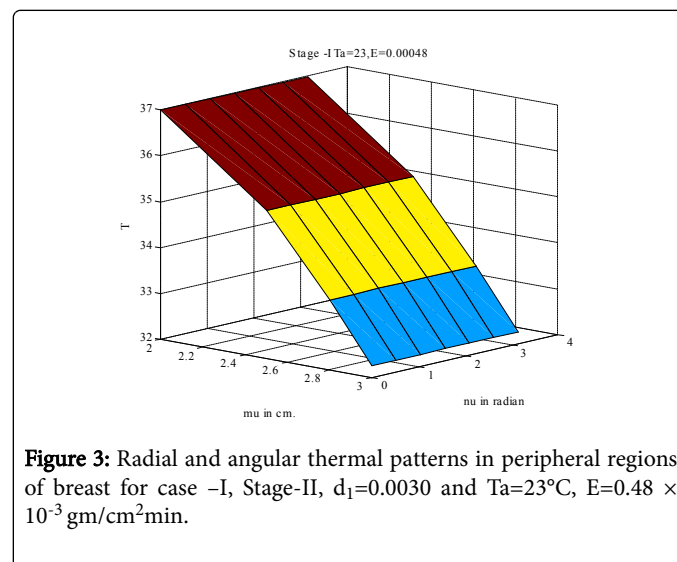


Figure 3: Radial and angular thermal patterns in peripheral regions of breast for case -I, Stage-II, $d_1=0.0030$ and $T_a=23^\circ C$, $E=0.48 \times 10^{-3}$ gm/cm²min.

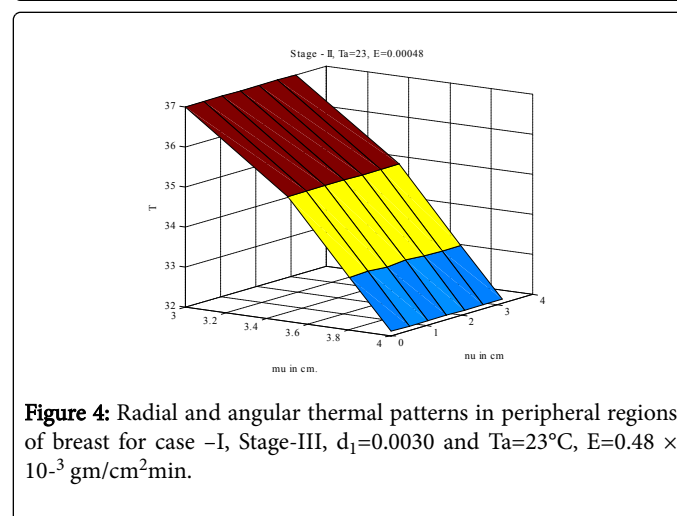


Figure 4: Radial and angular thermal patterns in peripheral regions of breast for case -I, Stage-III, $d_1=0.0030$ and $T_a=23^\circ C$, $E=0.48 \times 10^{-3}$ gm/cm²min.

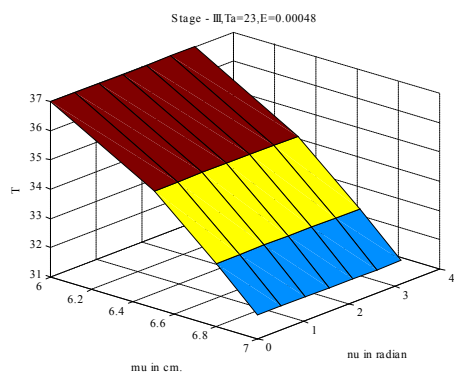


Figure 5: Radial and angular thermal patterns in peripheral regions of breast for case -I, Stage-IV, $d_1=0.0030$ and $T_a=23^\circ\text{C}$, $E=0.48 \times 10^{-3} \text{ gm/cm}^2\text{min}$.

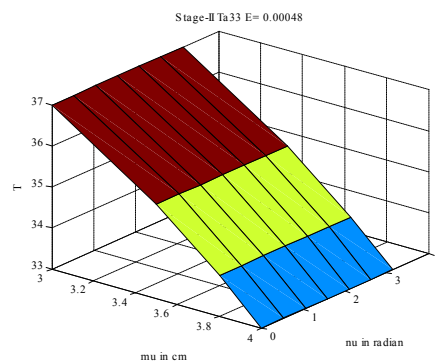


Figure 8: Radial and angular thermal patterns in peripheral regions of breast for case -I, Stage-III, $d_1=0.0030$ and $T_a=33^\circ\text{C}$, $E=0.48 \times 10^{-3} \text{ gm/cm}^2\text{min}$.

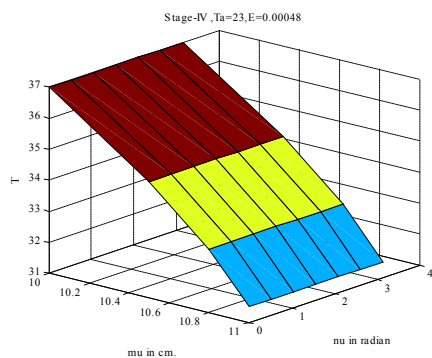


Figure 6: Radial and angular thermal patterns in peripheral regions of breast for case-I, Stage-V, $d_1=0.0030$ and $T_a=23^\circ\text{C}$, $E=0.48 \times 10^{-3} \text{ gm/cm}^2\text{min}$.

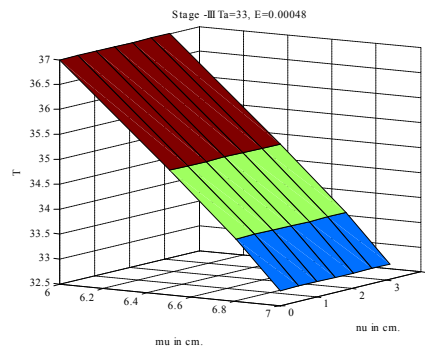


Figure 9: Radial and angular thermal patterns in peripheral regions of breast for case -I, Stage-IV, $d_1=0.0030$ and $T_a=33^\circ\text{C}$, $E=0.48 \times 10^{-3} \text{ gm/cm}^2\text{min}$.

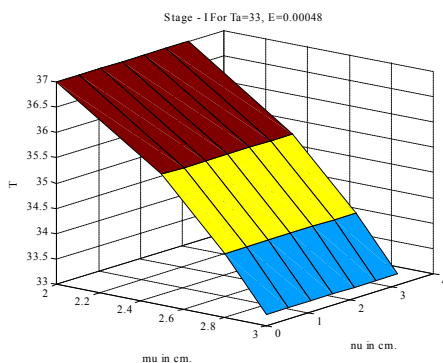


Figure 7: Radial and angular thermal patterns in peripheral regions of breast for case -I, Stage-II, $d_1=0.0030$ and $T_a=33^\circ\text{C}$, $E=0.48 \times 10^{-3} \text{ gm/cm}^2\text{min}$.

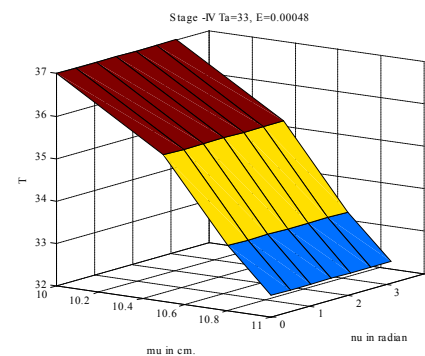


Figure 10: Radial and angular thermal patterns in peripheral regions of breast for case -I, Stage-V, $d_1=0.0030$ and $T_a=33^\circ\text{C}$, $E=0.48 \times 10^{-3} \text{ gm/cm}^2\text{min}$.

In these Figures it is also observed that the slope of the curve changes at junction of the different layers in the region. The temperature falls down as we move from breast core to the outer surface along radial direction. In Figure 10 for stage V it is observed

that the fall in temperature is more as compared to that in Figure 7 for stage II. This may be because the surface area of breast in stage V which is exposed to the environment is more as compared to that in stage II.

Figures 11 to 14 show the thermal patterns for $T_a=23^\circ\text{C}$, $E=0.48 \times 10^{-3} \text{ gm/cm}^2\text{min}$, case I and stage V for different eccentricities $d_1=0, 0.25, 0.5$ and 0.75 respectively. In Figure 14 for $d_1=0.75$ it is observed that the fall in the temperature is less as compared to Figure 11 for $d_1=0$.

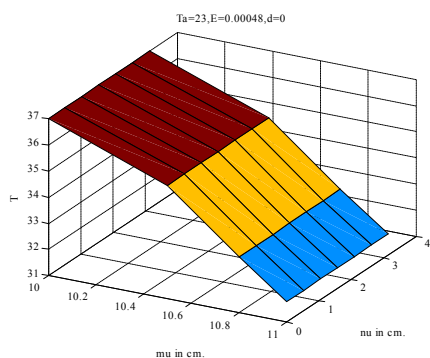


Figure 11: Radial and angular thermal patterns in peripheral regions of breast for case -I, Stage-V, $d_1=0.0$ and $T_a=23^\circ\text{C}$, $E=0.48 \times 10^{-3} \text{ gm/cm}^2\text{min}$.

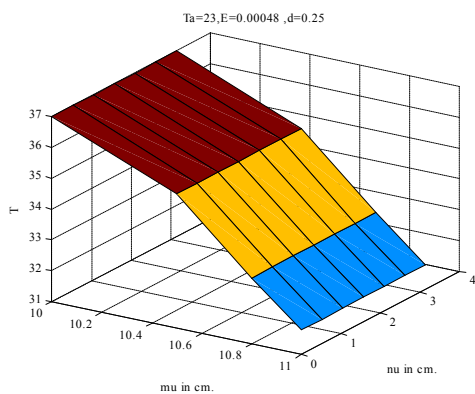


Figure 12: Radial and angular thermal patterns in peripheral regions of breast for case -I, Stage-V, $d_1=0.25$ and $T_a=23^\circ\text{C}$, $E=0.48 \times 10^{-3} \text{ gm/cm}^2\text{min}$.

Figures 15 to 18 show the thermal patterns for $T_a=33^\circ\text{C}$, $E=0.48 \times 10^{-3} \text{ gm/cm}^2\text{min}$, case I and stage V for different eccentricity $d_1=0, 0.25, 0.5$ and 0.75 respectively. In Figure 18 for $d_1=0.75$ it is observed that the fall in the temperature is less as compared to Figure 15 for $d=0$. This may be due to higher surface area of breast exposed to the environment for lower eccentricity $d_1=0$. Comparing Figures 3 to 10 with Figures 11 to 18, we observe that the fall in temperature is more at lower atmospheric temperature (i.e., $T_a=23^\circ\text{C}$) than that for higher atmospheric temperature (i.e., $T_a=33^\circ\text{C}$).

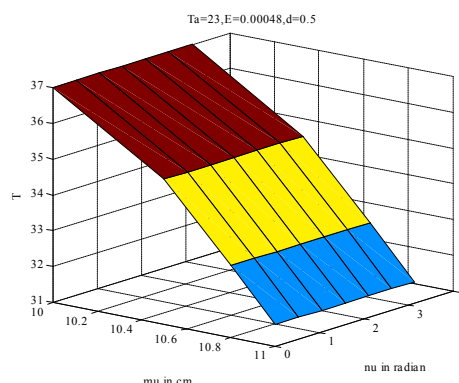


Figure 13: Radial and angular thermal patterns in peripheral regions of breast for case -I, Stage-V, $d_1=0.50$ and $T_a=23^\circ\text{C}$, $E=0.48 \times 10^{-3} \text{ gm/cm}^2\text{min}$.

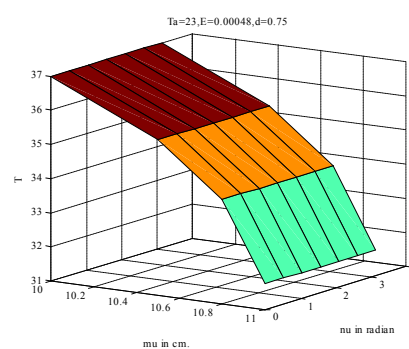


Figure 14: Radial and angular thermal patterns in peripheral regions of breast for case -I, Stage-V, $d_1=0.75$ and $T_a=23^\circ\text{C}$, $E=0.48 \times 10^{-3} \text{ gm/cm}^2\text{min}$.

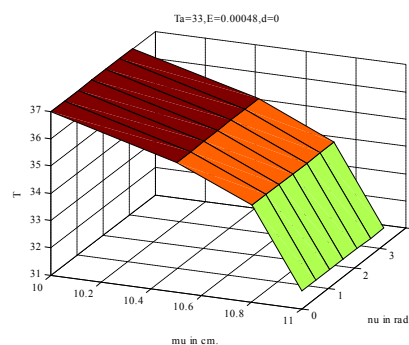


Figure 15: Radial and angular thermal patterns in peripheral regions of breast for case -I, Stage-V, $d_1=0.0$ and $T_a=33^\circ\text{C}$, $E=0.48 \times 10^{-3} \text{ gm/cm}^2\text{min}$.

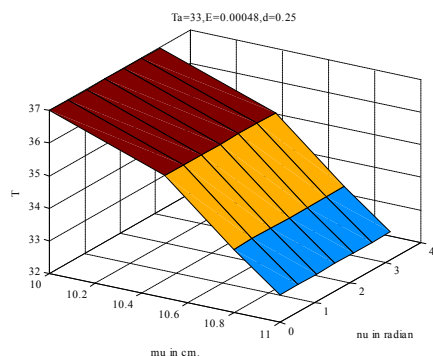


Figure 16: Radial and angular thermal patterns in peripheral regions of breast for case -I, Stage-V, $d_1=0.25$ and $T_a=33^\circ\text{C}$, $E=0.48 \times 10^{-3} \text{ gm/cm}^2\text{min}$.

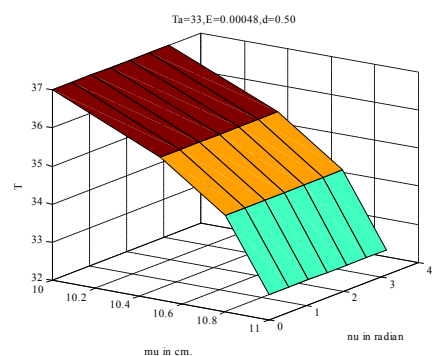


Figure 17: Radial and angular thermal patterns in peripheral regions of breast for case -I, Stage-V, $d_1=0.50$ and $T_a=33^\circ\text{C}$, $E=0.48 \times 10^{-3} \text{ gm/cm}^2\text{min}$.

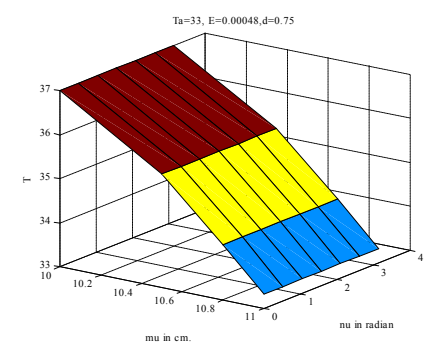


Figure 18: Radial and angular thermal patterns in peripheral regions of breast for case -I, Stage-V, $d_1=0.75$ and $T_a=33^\circ\text{C}$, $E=0.48 \times 10^{-3} \text{ gm/cm}^2\text{min}$.

It is not possible to present the graphs for all the different values of parameters involved. Therefore the results for different eccentricities based on stages of breast development, atmospheric temperature and for different rate of evaporations are presented in the Tables 2 to 7. We

observe in Tables 2 to 7 that surface area of the breast exposed to environment increases with the stages of development from stage II to V.

The Table 2 shows the nodal temperatures for $T_a=150^\circ\text{C}$, $E=0$, same eccentricity $d_1=0.0030$ and different stages of development of breast. The nodal temperature T_2 , T_3 and T_4 are higher for stage II and go on decreasing along with the stages III, IV and V. The maximum fall in nodal temperature is observed at the surface and the difference in T_4 between stages II and stage V is 0.30°C . The Table 3 shows the nodal temperatures for $T_a=23^\circ\text{C}$, $E=0.24 \times 10^{-3} \text{ gm/cm}^2\text{min}$, $E=0.48 \times 10^{-3} \text{ gm/cm}^2\text{min}$, same eccentricity $d_1=0.0030$ and different stages of development of breast. In Table 3 we observe that the nodal temperature T_2 , T_3 and T_4 decrease with the stages as we move from stage II to stage V. The difference in surface temperature for $T_a=23^\circ\text{C}$, $E=0.24 \times 10^{-3} \text{ gm/cm}^2\text{min}$ between stage II and stage V is 0.64°C . Again for $T_a=230^\circ\text{C}$, $E=0.48 \times 10^{-3} \text{ gm/cm}^2\text{min}$ the difference in surface temperature between stage II and stage V is 0.7518°C . In Table 3 we also observe that the difference in nodal temperatures between the stages increases with the increase in rate of evaporation.

Temperature	Stage-II	Stage-III	Stage-IV	Stage-V	Temperature difference between stages II & V
T1	37	37	37	37	0
T2	36.39	36.31	36.28	36.2	0.21
T3	35.512	35.45	35.4	35.305	0.307
T4	34.154	34.1509	34.0625	33.745	0.4091

Table 2: Nodal temperatures for $T_a=15$, $E=0$ Case-I and different stages of development of breast.

The Table 4 shows the nodal temperatures for $T_a=33^\circ\text{C}$, different values of rate of evaporation, same eccentricity $d_1=0.0030$, case I and different stages of development of breast. We observe that the nodal temperatures decrease with the stages, as we go from stage II to stage V. Also the nodal temperature in the different stages decrease with the increase in rate of evaporation. This is due to the fact that the surface area of breast increases with the stages of development and the surface area have the most significant effect on thermal patterns in the breast at the higher rate of evaporation because more heat loss takes place from outer surface to the environment due to higher rate of evaporation.

The Tables 5, 6 and 7 show the nodal temperatures due to different eccentricities and full matured stage (i.e., stage V) of the breast. The Table 5 shows the nodal temperatures for $T_a=15^\circ\text{C}$, $E=0$, different eccentricities $d_1=0.0, 0.25, 0.50, 0.75$, stage V of development of breast and case I. The nodal temperature T_2 , T_3 and T_4 are higher for $d_1=0.75$ and go on decreasing with decrease in eccentricity and ($d_1=0.5, 0.25$ and 0.0) the maximum fall in nodal temperature is observed at the surface and the difference in T_4 between $d_1=0$ and $d_1=0.75$ is 0.455°C . The Table 6 shows the nodal temperatures for $T_a=23^\circ\text{C}$, $E=0.24 \times 10^{-3} \text{ gm/cm}^2\text{min}$, $E=0.48 \times 10^{-3} \text{ gm/cm}^2\text{min}$, different eccentricities $d_1=0.0, 0.25, 0.50, 0.75$, stage V of development of breast and case I. In Table 6 we observe that the nodal temperature T_2 , T_3 and T_4 decrease with the eccentricities as we move from $d_1=0.75$ to $d_1=0$. The difference in surface temperature for $E=0.24 \times 10^{-3} \text{ gm/cm}^2\text{min}$ between $d_1=0.75$ and $d_1=0$ is 0.75°C . Again for $T_a=23^\circ\text{C}$,

$E=0.48 \times 10^{-3}$ gm/cm²min, the difference in surface temperature between $d_1=0.75$ to $d_1=0$ is 0.84°C. The Table 6 we observe that the difference in nodal temperatures due to different eccentricities increases with the increase in rate of evaporation.

Temperature		Stage-II	Stage-III	Stage-IV	Stage-V	Temperature difference between stages II & V
T1	$E=0.24 \times 10^{-3}$	37	37	37	37	0
T2		35.611	35.6502	35.45	35.2	0.4105
T3		34.659	34.6	34.385	34.15	0.5091
T4		33.825	33.5	33.25	33.185	0.64
T1	$E=0.48 \times 10^{-3}$	37	37	37	37	0
T2		35.226	35.12	35	34.75	0.476
T3		33.525	33.3	33.15	32.95	0.575
T4		32.252	32.1	31.8	31.5	0.7518

Table 3: Nodal temperatures for $T_a=23$, Case-I and different stages of development of breast.

Temperature		Stage-II	Stage-III	Stage-IV	Stage-V	Temperature difference between stages II & V
T1	$E=0.24 \times 10^{-3}$	37	37	37	37	0
T2		36.0255	36	35.75	35.56	0.4655
T3		35.3936	35.15	35	34.75	0.6436
T4		34.8446	34.7	34.5	34.05	0.7946
T1	$E=0.48 \times 10^{-3}$	37	37	37	37	0
T2		35.4775	35.3	35	34.75	0.7275
T3		34.2595	34	33.75	33.43	0.8295
T4		33.2207	33	32.75	32.25	0.9707
T1	$E=0.72 \times 10^{-3}$	37	37	37	37	0
T2		34.9295	34.8	34.5	34.1	0.8295
T3		33.1255	32.75	32.43	32.13	0.9955
T4		31.6967	31.35	31	30.55	1.1467

Table 4: Nodal temperatures for $T_a=33$, Case -I and different stages of development of breast.

Temperature	d=0	d=0.25	d=0.5	d=0.75	Temperature difference between eccentricities $d_1=0$ & 0.75
T1	37	37	37	37	0
T2	36.37	36.414	36.5	36.6546	0.2846
T3	35.3	35.45	35.51	35.626	0.326
T4	33.75	34.1	34.1546	34.205	0.455

Table 5: Nodal temperatures for $T_a=15$, $E=0$, Case-I, Stage V and different eccentricities.

Temperature		d=0	d=0.25	d=0.5	d=0.75	Temperature difference between eccentricities $d_1=0$ & 0.75
T1	$E=0.24 \times 10^{-3}$	37	37	37	37	0
T2		35.052	35.25	35.38	35.45	0.398
T3		34.05	34.15	34.28	34.585	0.535
T4		31.75	32.98	33.05	32.4	0.75
T1	$E=0.48 \times 10^{-3}$	37	37	37	37	0
T2		34.98	35	35.2	35.35	0.37
T3		33.65	33.5	33.75	34.35	0.7
T4		31.35	31.6	31.98	32.19	0.84

Table 6: Nodal temperatures for $T_a=23$, Case-I, Stage V and different eccentricities.

The Table 7 shows the nodal temperatures for $T_a=33^\circ\text{C}$, different values of rate of evaporation, different eccentricities $d_1=0.0, 0.25, 0.50, 0.75$, stage V of development of breast and case I boundary condition. We observe that the nodal temperatures decrease with the decrease in the eccentricities, as we go from $d_1=0.75$ to 0.0. Also the nodal temperature decreases with the increase in rate of evaporation. Further the difference in nodal temperatures due to different eccentricities increases with the increase in rate of evaporation.

This is due to the fact that the surface area of breast increases with the decrease in eccentricity and the surface area has the significant effect on thermal patterns in the breast at the higher rate of evaporation because as more heat loss takes place from the outer surface to the environment due to higher rate of evaporation.

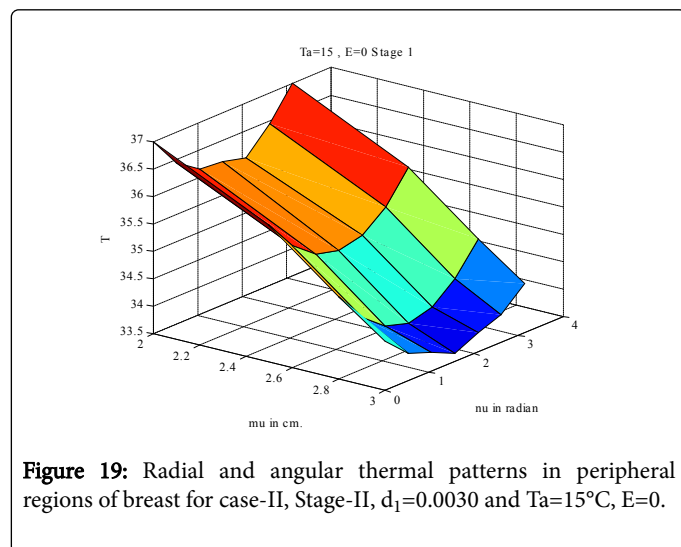
Temperature		d=0	d=0.25	d=0.5	d=0.75	Temperature difference between eccentricities $d_1=0$ & 0.75
T1	$E=0.24 \times 10^{-3}$	37	37	37	37	0
T2		35.5	35.65	36.05	36.0255	0.5255
T3		34.75	34.98	35.13	35.39	0.64

T4		34.22	34.35	34.65	34.944 6	0.7246
T1	E=0.48 $\times 10^{-3}$	37	37	37	37	0
T2		34.75	35.05	35.25 8	35.377 5	0.6275
T3		33.54	33.85	34	34.359 5	0.8195
T4		32.35	32.85	33.1	33.320 7	0.9707
T1	E=0.72 $\times 10^{-3}$	37	37	37	37	0
T2		34.3	34.75	34.98	35.029 5	0.7295
T3		32.22	32.9	33	33.125 5	0.9055
T4		30.75 2	31.12	31.32	31.895 6	1.1436

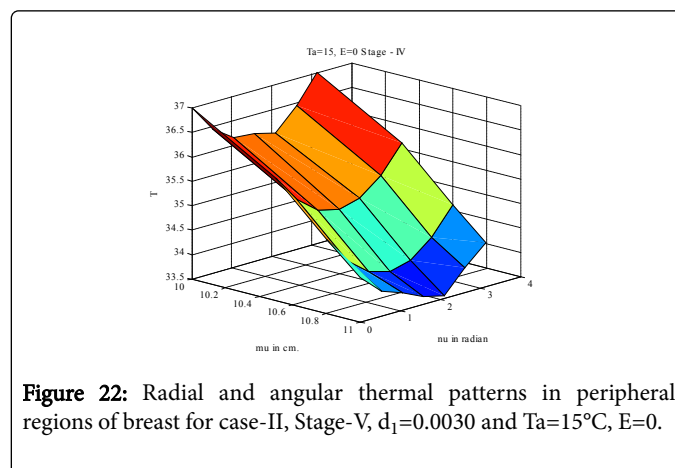
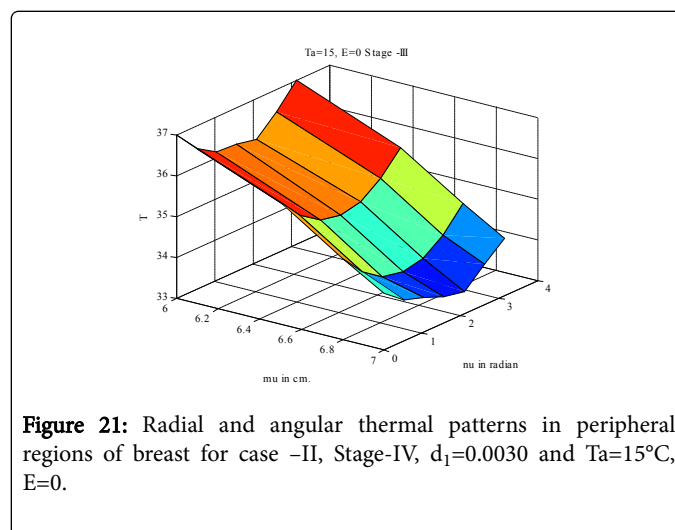
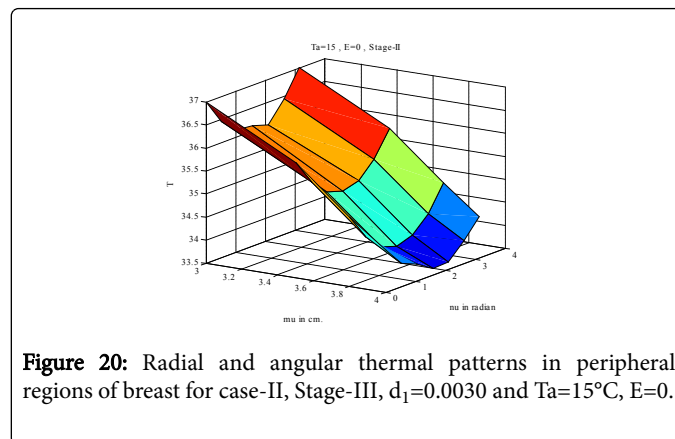
Table 7: Nodal temperatures for $T_a=33$, Case-I, Stage V and different eccentricities.

Case II boundary condition

Figures 19 to 22 show the radial and angular direction distribution in peripheral region of breast for case-II, eccentricity $d_1=0.0030$, $T_a=15^\circ\text{C}$, $E=0$ and stage-II, III, IV and V of breast development respectively. In these Figures the effect of parabolic variation of inner core temperature of breast is clearly visible on temperature profiles in peripheral region of breast. Also the slope of the curve changes at the different radial positions at the interfaces of layers of peripheral region. The fall in temperature along radial direction is more in Figure 22 as compared to that Figure 19. Thus due to higher surface area exposed to environment in the stage-V as compared to that in the stage-II.



Figures 23 to 26, show the radial and angular thermal patterns in peripheral region of breast for case-II, stage-V, $T_a=15^\circ\text{C}$, $E=0$ and $d_1=0.0, 0.25, 0.50, 0.75$ of breast respectively. The effect of parabolic variation on inner boundary temperature of breast is visible on temperature profiles of peripheral region of the breast.



The fall in temperature is more in Figure 23 as compared to that in Figure 26. Thus the fall in temperature decreases with increase in eccentricities. This is because the surface area decreases with increase in eccentricities.

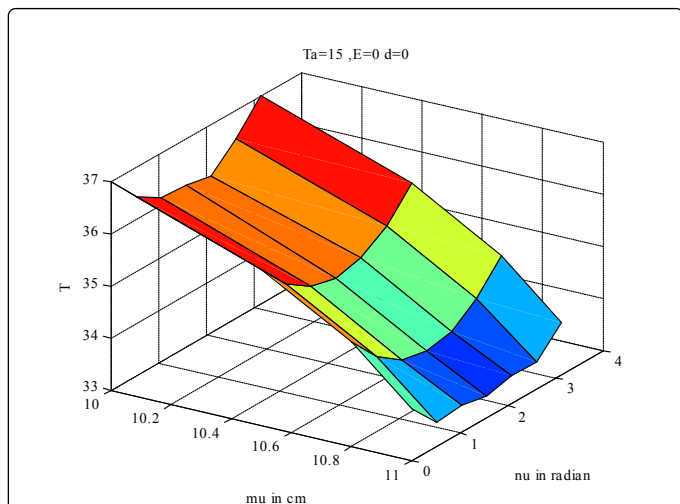


Figure 23: Radial and angular thermal patterns in peripheral regions of breast for case-II, Stage-V, $d_1=0.0$ and $T_a=15^\circ\text{C}$, $E=0$.

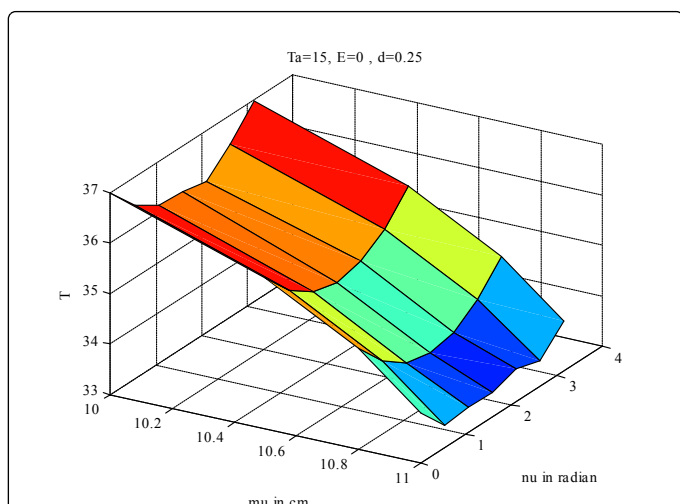


Figure 24: Radial and angular thermal patterns in peripheral regions of breast for case-II, Stage-V, $d_1=0.25$ and $T_a=15^\circ\text{C}$, $E=0$.

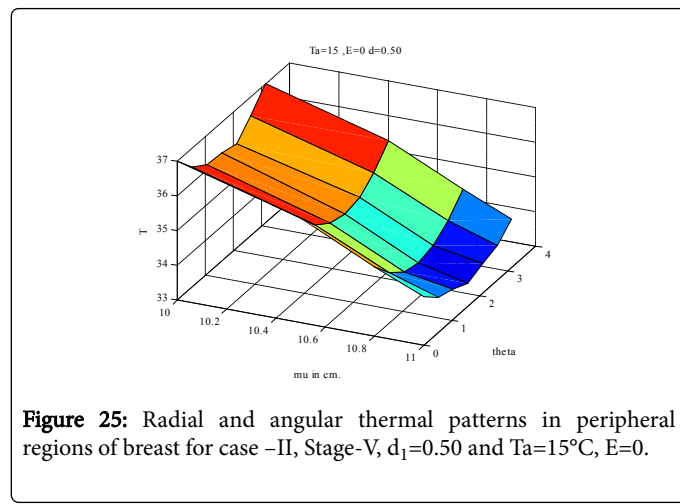


Figure 25: Radial and angular thermal patterns in peripheral regions of breast for case-II, Stage-V, $d_1=0.50$ and $T_a=15^\circ\text{C}$, $E=0$.

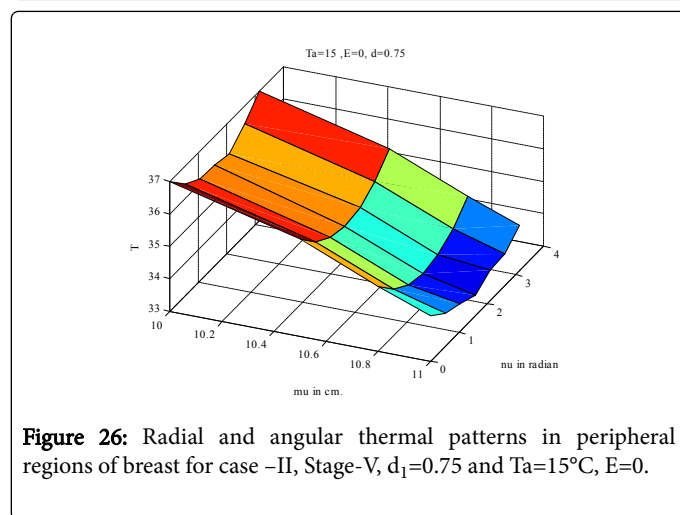


Figure 26: Radial and angular thermal patterns in peripheral regions of breast for case-II, Stage-V, $d_1=0.75$ and $T_a=15^\circ\text{C}$, $E=0$.

The Table 8 shows the values of nodal temperatures for $T_a=15^\circ\text{C}$, $E=0$, case-II, $d_1=0.0030$ and different stages of development of breast. We observe that the difference in nodal temperatures in the stages II to stage V increases as we move from breast core to breast surface. The nodal temperatures decrease as we move from stage II to stage V.

Table 9 shows nodal temperatures for $T_a=15^\circ\text{C}$, $E=0$, case-II, stage V and different eccentricities of breast.

Temperature	Stage-II			Stage-III			Stage-IV			Stage-V			Temperature difference between stages II & V		
	$\Theta=0$	$\Theta=\pi/2$	$\Theta=\pi$	$\Theta=0$	$\Theta=\pi/2$	$\Theta=\pi$	$\Theta=0$	$\Theta=\pi/2$	$\Theta=\pi$	$\Theta=0$	$\Theta=\pi/2$	$\Theta=\pi$	$\Theta=0$	$\Theta=\pi/2$	$\Theta=\pi$
T1	37	36	37	37	36	37	37	36	37	37	36	37	0	0	0
T2	36.5	35.5	36.5	36.3	35.3	36.3	36.3	35.28	36.3	36.3	35.2	36.3	0.2	0.3	0.2
T3	35.5	34.73	35.5	35.4	34.6	35.4	35.3	34.5	35.3	35.2	34.3	35.2	0.31	0.43	0.32
T4	34.2	33.75	34.2	34.1	33.55	34.1	34.1	33.45	34.1	33.8	33.2	33.8	0.45	0.55	0.45

Table 8: Nodal temperatures for $T_a=15$, $E=0$ Case-II and different stages of development of breast.

In Table 9 we observe that the difference in nodal temperatures for eccentricities 0 and 0.75 increase as we move from breast core towards the surface of the breast. Also the nodal temperature increases with the increase in eccentricities. This is due to decrease in surface area of breast with increase in eccentricity thereby reducing the heat loss from surface to the environment due to conduction, convection radiation and evaporation.

The present model can be used to obtain the similar results for different cases of atmospheric temperatures. The model is valid for higher atmospheric temperature up to 45°C and lower atmospheric temperature up to 5°C. But for freezing temperature below 5°C model has to be modified for cold injuries. For higher atmospheric

temperature above 45°C the present model has to be modified for heat/burn injuries. The model can further be modified and extended for the problem involving abnormalities like cancer to generate the temperature profiles for patients suffering from cancer. The temperature profile for abnormal case (cancer) can be compared with those for normal case to identify the location of differences of temperature profiles which in turn can be used to detect the location of abnormalities like cancer. Further the models can be simulated for different size and type of tumors to generate the temperature profiles. This thermal information can again be used to compare with normal profiles to detect size and type of tumor.

Temperature	d=0			d=0.25			d=0.5			d=0.75			Temperature difference between eccentricities 0 & 0.75		
	$\Theta=0$	$\Theta=\pi/2$	$\Theta=\pi$	$\Theta=0$	$\Theta=\pi/2$	$\Theta=\pi$	$\Theta=0$	$\Theta=\pi/2$	$\Theta=\pi$	$\Theta=0$	$\Theta=\pi/2$	$\Theta=\pi$	$\Theta=0$	$\Theta=\pi/2$	$\Theta=\pi$
T1	37	36	37	37	36	37	37	36	37	37	36	37	0	0	0
T2	36.3	35.2	36.3	36.48	35.28	36.48	36.5	35.3	36.5	36.55	35.5	36.55	0.25	0.3	0.25
T3	35.3	34.09	35.29	35.4	34.2	35.4	35.55	34.4	35.55	35.61	34.53	35.61	0.31	0.44	0.32
T4	33.75	33.19	33.75	34.06	33.45	34.06	34.1	33.55	34.15	34.2	33.75	34.17	0.45	0.56	0.45

Table 9: Nodal temperatures for $T_a=15$, $E=0$, Case-II, Stage V and different eccentricities.

Conclusions

A two dimensional finite element model is proposed and employed to study the thermal patterns in the peripheral regions of human breast for a steady state case. The coaxial elliptical sectoral elements are employed in finite element discretization of the region to effectively incorporate the variation in parameters due to non homogeneity of skin and subdermal tissues of human breast. The model gives the result with high accuracy of 99.89% and these results are in agreement with the biological facts. However no theoretical or experimental results on thermal patterns in elliptical shaped human organs are available for comparison. The coaxial elliptical sectoral elements based finite element approach has been effectively used to model the realistic semi elliptical shaped of human breast varying in shape and size in terms of eccentricity, radius of minor and major axes due to different stages of breast developments. The present model is the most realistic model in terms of the shape and size in comparison to the models reported in the literature for the study of thermal patterns in human breast. On the basis of results it is concluded that the surface area of breast exposed to the environment changes with the changes in eccentricity due to different stages of development and it causes significant change in the thermal patterns of human breast. This thermal information of human breast due to change in shape and size of breast is of crucial importance in thermography for distinguishing the change in thermograms due to shape and size of breast and tumours. Further it can be concluded that the atmospheric temperature and rate of evaporation have significant effect on thermal patterns in human breast and this effect changes significantly with the change in shape and size of the breast. Finally the different stages of development of breast exhibit different thermal behaviours. The thermal information generated from such models can be useful for developing the strategy for thermography in relevance to atmospheric temperature,

evaporation rates, shape and size of human breast for detection of breast cancer.

References

1. Agrawal M, Adlakha N, Pardasani KR (2010) Semi numerical Model to Study Thermal patterns in Peripheral Layers of Elliptical and Tapered Shaped Human Limbs. *J Mech in Medicine and Biology* 10: 57-72.
2. Agrawal M, Adlakha N, Pardasani KR (2010) Three Dimensional Finite Element Model to study heat flow in Dermal Region of elliptical and tapered shaped human limbs. *Applied Mathematics and Computations* 217: 4129-4140.
3. Agrawal M, Adlakha N, Pardasani KR (2010) Thermal disturbances in dermal regions of human limbs involving metastasis of tumors. *International Mathematical Forum* 5: 1903-1914.
4. Gurung DB (2009) FEM approach to one dimensional unsteady thermal patterns in human dermal parts with quadratic shape function. *J Appl Math & Informatics* 27: 301-303.
5. Gurung DB (2010) Transient thermal patterns in human dermal part with protective layer at low atmospheric temperature. *International Journal of Biomathematics* 3: 439-451.
6. Saxena VP, Bindra JS (1984) Steady state thermal patterns in dermal regions of human body with variable blood flow perspiration and self controlled metabolic heat generation. *Indian J Pure Appl Math* 15: 31-42.
7. Gonzalez FJ (2007) Thermal simulation of breast tumors. *Revista Mexicana de Fisica* 53: 323-326.
8. Ghizzoni L, Beccuti G (2011) Normal and Abnormal Puberty.
9. Saxena VP, Arya D (1981) Steady state heat distribution in epidermis, dermis and sub dermal tissue. *J Theor Biol* 89: 423-432.
10. Saxena VP, Arya D (1981) Exact solution of thermal patterns problem in epidermis and dermis regions of human body. *Proc VNM Medical and Biological Engineering, Sweden*.
11. Saxena VP (2013) Thermal patterns in human skin and sub dermal tissues. *J Theor Biol* 102: 277-286.

12. Saxena VP, Pardasani KR (1991) Effect of dermal tumor on thermal patterns in skin with variable blood flow. *Bull Mathematical Biology, USA*.
13. Pardasani KR, Adlakha N (1991) Exact solution to a heat flow problem in peripheral tissue layers with a solid tumor in the dermis. *Indian Journal pure applied math* 22: 679-687.
14. Pardasani KR, Shakya M (2005) A two dimensional infinite element model to study Thermal patterns in human dermal regions due to tumors. *Journal of Mathematics and Statistics* 1: 184-188.
15. Pardasani KR, Shakya M (2008) Infinite element thermal model for human dermal regions with tumors. *Int Journal of Applied Sc & Computations* 15: 1-10.
16. Pardasani KR, Saxena VP (1989) Exact solution to thermal patterns problem in Annular Skin Layers. *Bull Calcutta Math Soc* pp: 81-108.
17. Pardasani KR, Adlakha N (1993) Two dimensional Steady State Thermal patterns in Annular Tissues of a human or animal body. *Ind J Pure Applied Math* 24: 721-728.
18. Pardasani KR, Adlakha N (1995) Coaxial circular sector elements to study two- dimensional heat distribution problem in dermal regions of human limbs. *Math & Comp Modelin* 22: 127-140.
19. Khanday MA, Saxena VP (2009) Finite element approach for the study of thermoregulation in human head exposed to cold environment. *Proceedings Journal of American Institute of Physics* 1146: 375-385.
20. Osman MM, Afify EM (1984) Thermal modelling of the normal woman's breast. *J Biomech Engg* 106: 123-130.
21. Osman MM (1994) Effect of arterio- venous heat exchange on breast temperature profile. *J Phys III France* 4: 435-442.
22. Osman MM, Afify EM (1988) Thermal modelling of the malignant woman's breast. *J Biomech Engg* 110: 269- 276.
23. Sudharsan NM, Ng EYK, Teh SL (1999) Surface thermal patterns of a breast with and without tumor. *Comput Methods Biomech Biomed Engin* 23: 187-199.
24. Das TK, Sangodkar J, Negre N, Narla G, Cagan RL (2013) Sin3a acts through a multi-gene module to regulate invasion in *Drosophila* and human tumors. *Oncogene* 32: 3184-3197.
25. Agrawal M, Adlakha N, Pardasani KR (2009) Two dimensional thermal distribution model in dermal layers of elliptical shaped human limbs involving a uniformly perfused tumor. *International Journal of Computational and Applied Mathematics* 4: 29-40.
26. Agrawal M, Adlakha N, Pardasani KR (2011) Finite Element Model to study Thermal Effect of Uniformly Perfused Tumor in Dermal layers of Elliptical Shaped Human Limbs. *Int J Biomathematics* 4: 241-254.
27. Agrawal M, Adlakha N, Pardasani KR (2014) Steady state temperature distribution in dermal regions of an irregular tapered shaped human limb with variable eccentricity. *Journal of Thermal Biology* 44: 27-34.
28. Agrawal M, Adlakha N, Pardasani KR (2015) Finite element model to study the thermal effect of tumors in dermal regions of irregular tapered shaped human limbs. *International Journal of Thermal Sciences* 98: 287-295.
29. Agrawal M, Adlakha N, Pardasani KR (2016) Finite Element Model to Study Temperature Distribution in Skin and Deep Tissues of Human Limbs. *Journal of Thermal Biology*.
30. Makrariya A, Adlakha N (2013) Two-dimensional finite element model of thermal patterns in dermal tissues of extended spherical organs of a human body. *International Journal of Biomathematics* 6: 1250065-1-1250065-15
31. Makrariya A, Adlakha N (2015) Two Dimensional Finite Element Model to Study Thermal patterns in Peripheral Regions of Extended Spherical Human Organs Involving Uniformly Perfused Tumors. *International Journal of Biomathematics* 8: 1550074-15500104
32. Makrariya A, Adlakha N (2015) Thermal Stress Due to Tumor in Periphery of Human Breast. *Open Science Journal of Bioscience and Bioengineering* 2: 50-59.
33. Perl W (1963) Heat and matter distribution equation to include clearance by capillary blood flow. *Ann NY Acad Sc* 108: 92-105.